Bull. Mater. Sci., Vol. 32, No. 3, June 2009, pp. 231–237. © Indian Academy of Sciences.

Magnetic and photocatalytic properties of nanocrystalline $ZnMn_2O_4$#

MENAKA, MOHAMMED QAMAR, SAMUEL E LOFLAND†, KANDALAM V RAMANUJACHARY†† and ASHOK K GANGULI*

Department of Chemistry, Indian Institute of Technology, New Delhi 110 016, India
†Department of Physics and Astronomy,
††Department of Chemistry and Biochemistry, Rowan University, Glassboro, NJ-08028, USA

Abstract. **The present study describes the synthesis of $ZnMn_2O_4$ nanoparticles with the spinel structure. These oxide nanoparticles are obtained from the decomposition of metal oxalate precursors synthesized by (a) the reverse micellar and (b) the coprecipitation methods. Our studies reveal that the shape, size and morphology of precursors and oxides vary significantly with the method of synthesis. The oxalate precursors prepared from the reverse micellar synthesis method were in the form of rods (micron size), whereas the coprecipitation method led to spherical nanoparticles of size, 40–50 nm. Decomposition of oxalate precursors at low temperature (~450°C) yielded phase pure $ZnMn_2O_4$ nanoparticles. The size of the nanoparticles of $ZnMn_2O_4$ obtained from reverse micellar method is relatively much smaller (20–30 nm) as compared to those made by the co-precipitation (40–50 nm) method. Magnetic studies of nanocrystalline $ZnMn_2O_4$ confirm antiferromagnetic ordering in the broad range of ~150 K. The photocatalytic activity of $ZnMn_2O_4$ nanoparticles was evaluated using photo-oxidation of methyl orange dye under UV illumination and compared with nanocrystalline TiO_2.**

Keywords. **Nanostructures; chemical synthesis; electron microscopy.**

1. Introduction

Zinc manganese oxide, with spinel-like structure has attracted much attention because of its tremendous technological importance as catalysts (Bessekhaud *et al* 2005), solid electrolytes (Yang *et al* 1996), negative temperature coefficient (NTC) thermistor (Fritsch *et al* 2000) and as sensor materials (Sorita and Kawano 1996). $ZnMn_2O_4$ has a normal spinel structure with a tetragonal distortion (c/a = 1·14) of the face centred pseudocubic cell having cell parameters of a = 8·087 and c = 9·245 Å (Asbrink *et al* 1999). The distortion (Jahn–Teller type) causes instability of the Mn^{+3} ion located at the octahedral site within the oxygen sublattice. Micron-sized particles of $ZnMn_2O_4$ have been prepared earlier by various methods like sol–gel (Monros *et al* 1995), solid-state reaction (Chhor *et al* 1986; Feltz and Jager 1988; Peiteado *et al* 2007; El-Aiashy *et al* 1995) and coprecipitation methods (Rosenberg *et al* 1963). Zhang *et al* (2007) synthesized $ZnMn_2O_4$ nanoparticles of size 20–50 nm by a hydrothermal method, which requires 118 h (long time) for its completion. However, the above synthetic approaches do not have sufficient control on the size and morphology of the nanoparticles.

The reverse micellar route is known to facilitate the control of size and morphology of various nanoparticles (Ahmad *et al* 2004, 2005; Ganguli *et al* 2007). The present study describes the synthesis of nanocrystalline $ZnMn_2O_4$ by two methodologies, (i) reverse micellar and (ii) coprecipitation method. In the reverse micellar method, a microemulsion system consisting of an oil phase, a surfactant and an aqueous phase are mixed appropriately to give a thermodynamically stable isotropic dispersion of aqueous phase in a continuous oil phase (Luisi and Straub 1984; Fang *et al* 1997). The size of the aqueous droplets (reverse micelles) is in the range of 5–20 nm and hence lead to an optically transparent microemulsion (Kuiry and Seal 2004). On mixing the two microemulsions, precipitation takes place due to the collision of the droplets containing the reactants. The reverse micellar route is of importance since it provides a convenient way to synthesize nanosized and nearly mono-dispersed nanoparticles. Various authors have reported the magnetic behaviour of $ZnMn_2O_4$ which shows the presence of antiferromagnetism in $ZnMn_2O_4$ with a broad variation in the Neel temperature (Aiyama 1966; Chhor *et al* 1986; Asbrink *et al* 1999). The origin of such variation is, however, not very clear. Asbrink *et al* (1999) reported a Neel temperature of 21·5 K (magnetic moment = 4·9 μ_B/Mn) while Aiyama (1966) claimed the Neel temperature to be around 250 K. The unusually high Neel temperature of $ZnMn_2O_4$ could not be determined accurately using the susceptibility ($\chi - T$) curve but was obtained using specific heat measurement (Aiyama 1966).

*Author for correspondence (ashok@chemistry.iitd.ernet.in)
#Dedicated to Prof. C N R Rao on his 75th birthday

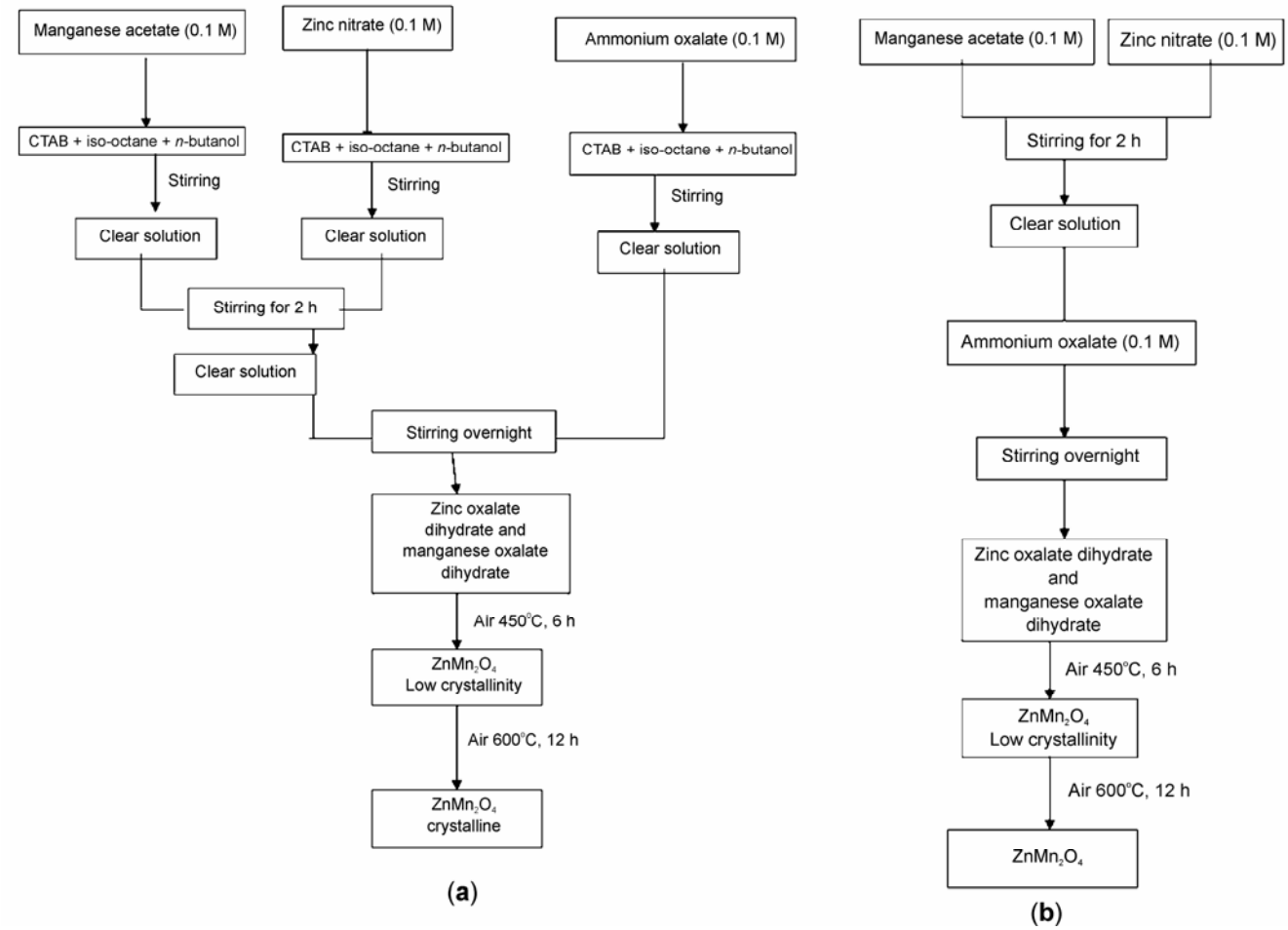

Figure 1. Flow chart indicating the method of synthesis of $ZnMn_2O_4$ using (**a**) reverse micellar method and (**b**) coprecipitation method.

Here we report the synthesis of rod-shaped zinc and manganese oxalate dihydrates (reverse micellar method) as well as spherical particles (coprecipitation method). Their decomposition yields pure $ZnMn_2O_4$ nanoparticles. The rods and nanoparticles have been characterized by powder X-ray diffraction (PXRD), thermogravimetric analysis (TGA), differential thermal analysis (DTA) and transmission electron microscopy (TEM). The magnetic behaviour of $ZnMn_2O_4$ nanoparticles was investigated using a Quantum Design Physical Properties Measurement system. The photocatalytic activity of $ZnMn_2O_4$ was evaluated spectrophotometrically (Bessekhaud *et al* 2005; Qamar *et al* 2008).

2. Experimental

We attempted to synthesize the mixed metal oxalate precursor, $ZnMn_2(C_2O_4)_3{\cdot}xH_2O$, by the reverse micellar method following the procedure developed earlier for other oxalates (Ahmad *et al* 2004, 2005). Three microemulsions were prepared using cetyltrimethyl ammonium bromide (CTAB) as the surfactant, 1-butanol as the co-surfactant, isooctane as the non-polar phase and the aqueous solutions were made up of 0·1 M of (i) zinc nitrate, (ii) manganese acetate and (iii) ammonium oxalate. The Zn^{+2} : Mn^{+2} molar ratio of 1 : 2 was maintained in the starting reagents. The weight fraction of various constituents in the microemulsions was 16·86% of CTAB, 14·1% of *n*-butanol, 58·91% of isooctane and 10·11% of aqueous phase. The synthetic procedure (reverse micellar method) for the synthesis of oxalate precursor as well as oxide nanoparticles is summarized in a flow chart (figure 1a).

We have also synthesized the mixture of oxalates of zinc and manganese by the coprecipitation method using ammonium oxalate and mixture of manganese acetate and zinc nitrate. 10 ml of 0·1 N aq. zinc nitrate solution was slowly mixed with 20 ml of 0·1 N aq. manganese acetate. To this solution 30 ml of 0·1 N ammonium oxalate was slowly added and then stirred overnight. The oxide nanoparticles were obtained after decomposition of the

precursors of zinc and manganese oxalate at a temperature of 450°C in air and to improve the crystallinity, further heated the sample at 600°C in air for 12 h.

Powder X-ray diffraction studies were carried out on a Bruker D8 Advance diffractometer with Ni-filtered Cu-Kα radiation using a step size of 0·02° and a step time of 1 s. Raw data were subjected to background correction and Kα2 lines were removed. The crystallite size was calculated from Scherrer's formula (Ahmad *et al* 2004). Thermogravimetric (TGA) and differential thermal analysis (DTA) experiments were carried out on a Perkin Elmer TGA and DTA system on well ground samples in a flowing nitrogen atmosphere with a heating rate of 5°C/min. Transmission electron microscopy (TEM) studies were carried out using a Tecnai G^2 20 electron microscope operated at 200 kV. TEM specimens were prepared by dispersing the oxide powder in ethanol by ultrasonic treatment. A few drops were poured onto a porous carbon film supported on a copper grid and then dried in air. Temperature and field dependent magnetization measurements were carried out at temperatures ranging from 5–300 K in an applied field of 1 kOe with a Quantum Design Physical Properties Measurement system.

The photocatalytic activity of $ZnMn_2O_4$ was evaluated with a photo-reactor made up of Pyrex glass equipped with a magnetic stirring bar. For irradiation experiments, 200 ml of methyl orange dye of 0·5 mM concentration was taken into the vessel and appropriate amount of the catalyst, ca 180 mg, of commercially available TiO_2 nanopowder (Aldrich, 99·7%) of ~5 nm size and 20 mg of

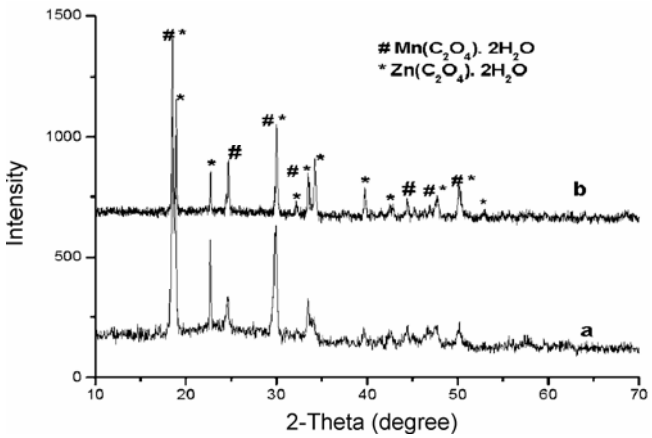

Figure 2. PXRD pattern of the metal oxalates obtained using a. reverse micellar and b. coprecipitation route.

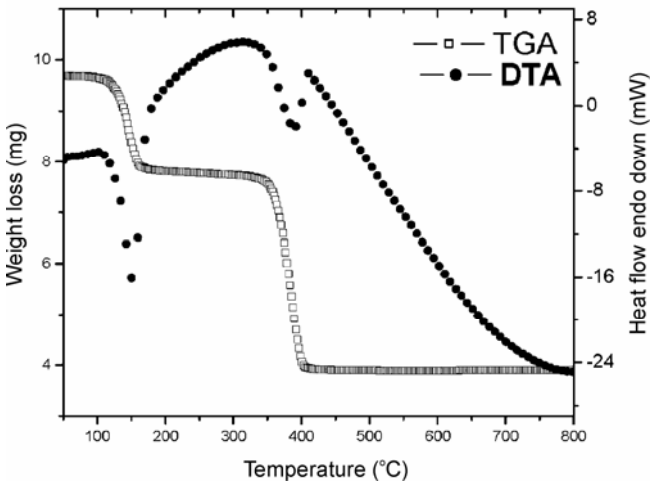

Figure 3. TGA/DTA plot for the decomposition of mixture of zinc oxalate and manganese oxalate prepared using reverse micellar route.

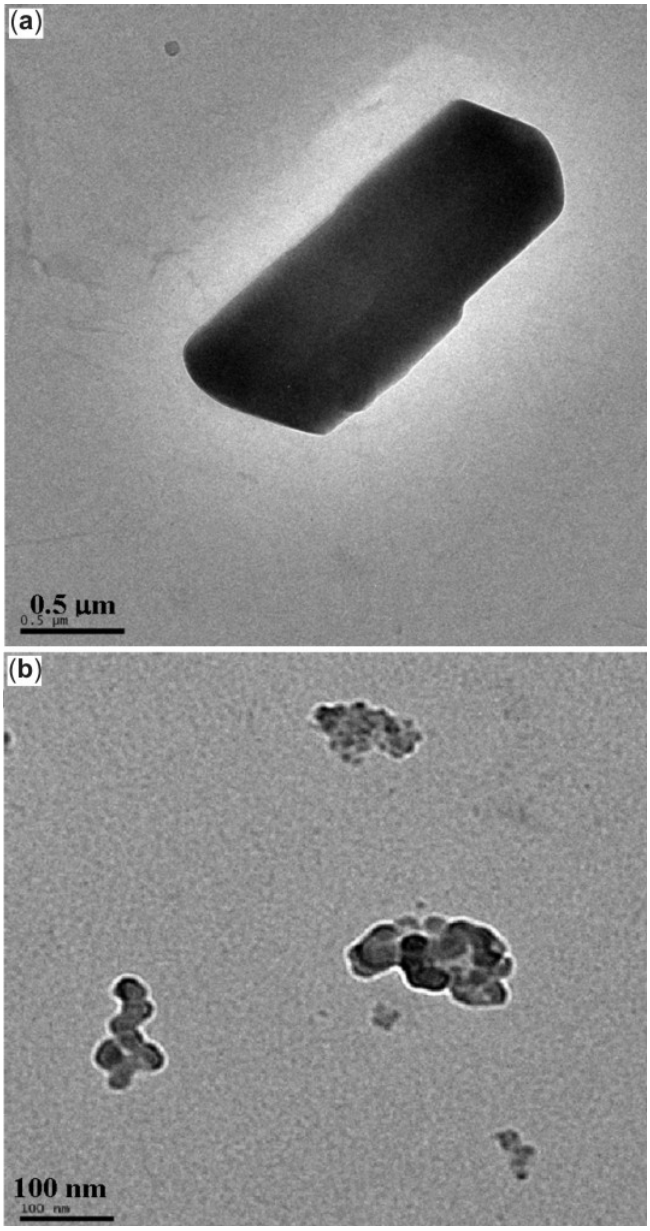

Figure 4. TEM image of the metal oxalates synthesized using (**a**) reverse micellar and (**b**) coprecipitation route.

$ZnMn_2O_4$ of ~25 nm size was added into the solution. Before irradiation, the solution was stirred for 15 min to allow the equilibration of the system so that the loss of methyl orange due to adsorption can be taken into account. The zero time reading was obtained from the blank solution kept in dark and then the solution was irradiated. Irradiation was carried out with a medium pressure mercury lamp and the samples were collected before irradiation and at regular interval during irradiation (Qamar *et al* 2008). The decrease in absorption intensity of the peak at 463 nm for the dye (0·5 mM), on irradiation with time was monitored by measuring the change in absorbance using a UV-Vis spectrophotometer. The same experiment was carried out using pure TiO_2 as well as pure $ZnMn_2O_4$ nanoparticles.

3. Results and discussion

The powder X-ray diffraction pattern of the precursor obtained by the reverse micellar method shows a mixture of manganese oxalate dihydrate and zinc oxalate dihydrate (figure 2a). The coprecipitation route also led to the formation of a mixture of the two oxalates (figure 2b). TGA of the oxalate precursor obtained from reverse micelle and coprecipitation method, shows two weight losses, the first weight loss is at around 140°C which corresponds to the loss of water molecule whereas the second weight loss is around 390°C and corresponds to the loss of CO and CO_2, leading to the conversion of the oxalates to $ZnMn_2O_4$. The DTA studies also showed two endotherms corresponding to decomposition of the mixed oxalate precursors (figure 3).

Transmission electron microscopy of the oxalate precursor obtained by the reverse micellar method showed the formation of micron-sized rods (figure 4a). Several

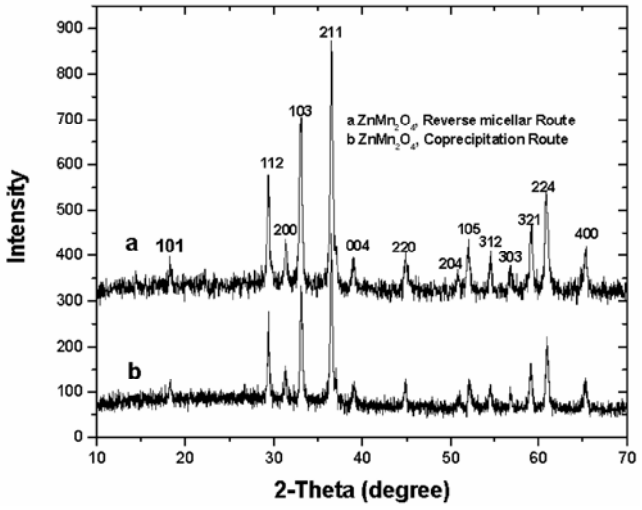

Figure 5. PXRD pattern of $ZnMn_2O_4$ synthesized at 600°C via **a**. reverse micellar and **b**. coprecipitation method.

transition metal carboxylates have shown the rod shaped morphology when synthesized using CTAB as a surfactant (Ahmad *et al* 2004, 2005; Ganguli *et al* 2007). The average dimension of the rods was 0·75 μm (diameter) and 2 μm (length) (figure 4a). However, transmission electron microscopy of the oxalate precursor obtained using the coprecipitation route showed the formation of uniform nanoparticles in the range of 40–50 nm (figure 4b). The oxalates were calcined at 450°C for 6 h to obtain $ZnMn_2O_4$. The powder X-ray pattern of $ZnMn_2O_4$ (figure 5a) was indexed on the basis of a tetragonal cell with lattice parameters $a = b = 5{\cdot}709(1)$ and $c = 9{\cdot}238(4)$ Å which is close to the reported lattice parameters of $ZnMn_2O_4$ (JCPDS 77-0470). From the refined lattice parameters it was observed that the $ZnMn_2O_4$ obtained via reverse micellar route was free from the mixed valence state of manganese cation (only Mn^{3+} ion is present). The c/a ratio is 1·618 which is very close to the c/a ratio calculated for the single crystal of $ZnMn_2O_4$ (Sorita and Kawano 1996). The crystallite size evaluated from X-ray line broadening was found to be ~25 nm which is in close agreement with the particle size (20–30 nm) obtained from transmission electron microscopic (figure 6a) studies. HRTEM studies show the lattice fringes and confirm the single crystalline nature of the nanoparticles (figure 6b). Monophasic $ZnMn_2O_4$ was also synthesized by decomposing the mixture of zinc oxalate and manganese oxalate obtained by coprecipitation method. The average crystallite size was evaluated from X-ray line broadening and was found to be ~40–50 nm which is in good agreement with the particle size (40–50 nm) obtained from the transmission electron microscopic studies (figure 7).

The magnetic properties of pure $ZnMn_2O_4$ (obtained by reverse micellar route) have been studied. The magnetization shows a broad transition at ~150 K signalling the onset of anti-ferromagnetic ordering in this phase. This temperature falls well within the range of Neel temperatures reported in the literature (figure 8). No effective magnetic moment calculations were attempted in view of the broad and complicated magnetic transition, but the results are similar to Aiyama *et al* (1966) bulk $ZnMn_2O_4$.

The photocatalytic activity of $ZnMn_2O_4$ prepared by reverse micelles has been investigated by photo-oxidation of methyl orange dye as the probe molecule. The degradation of methyl orange dye in the presence of $ZnMn_2O_4$ (without TiO_2) revealed that the absorbance of the contaminants remains more or less similar; however, a marked degradation of the dye was observed in the presence of 10% $ZnMn_2O_4 + TiO_2$ (anatase ~5 nm), as illustrated in figures 9a–c. The rate of degradation of methyl orange observed in the reaction with the mixture ($ZnMn_2O_4$ and TiO_2) was low as compared to that of pure TiO_2 (figure 9a). It is believed that the conduction band of $ZnMn_2O_4$ is higher (oxidation potential = +0·062 eV) than that of TiO_2 (oxidation potential ~ –0·5 eV) (Bessekhaud *et al*

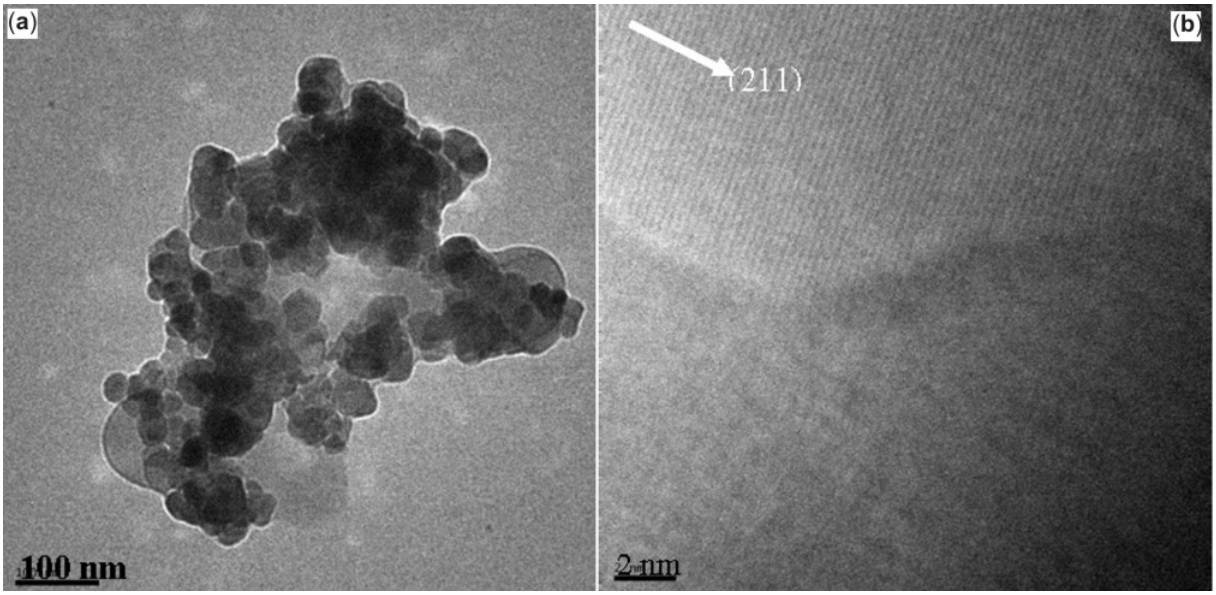

Figure 6. (**a**) TEM and (**b**) HRTEM image of $ZnMn_2O_4$ nanoparticles calcined at 600°C (using reverse micellar route).

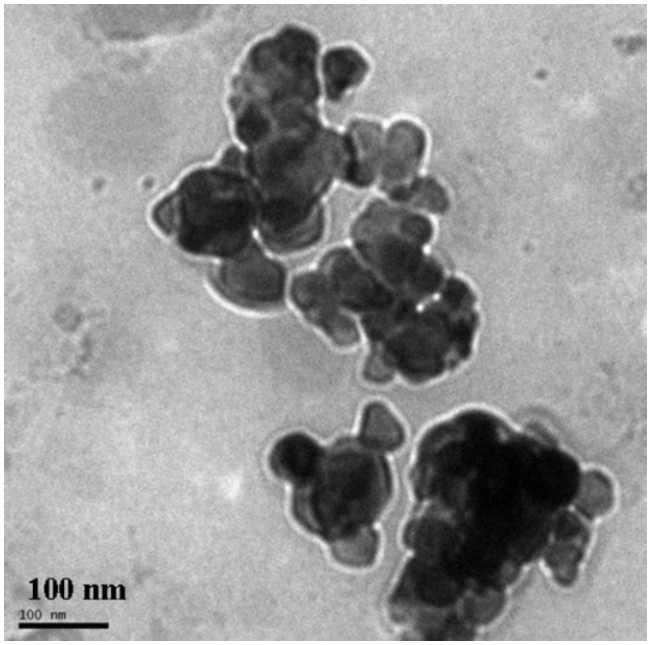

Figure 7. TEM images of $ZnMn_2O_4$ spherical nanoparticles synthesized at 600°C by coprecipitation method.

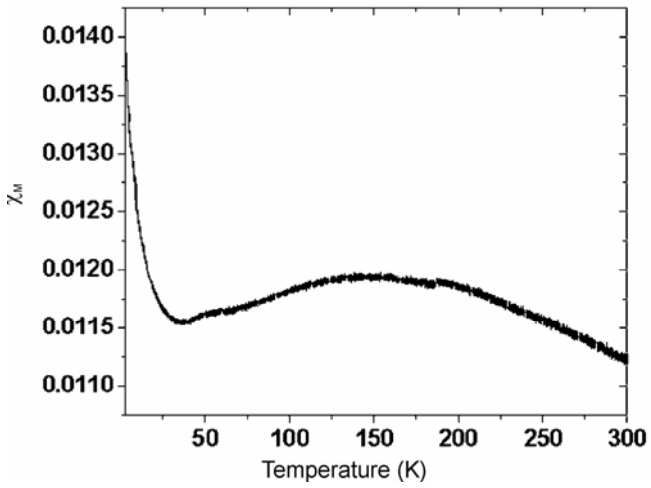

Figure 8. Plot of magnetic susceptibility of $ZnMn_2O_4$ with temperature.

2005) as shown in figure 10a, so the electron generated in the conduction band of $ZnMn_2O_4$ cannot be transferred to the corresponding band of TiO_2. Instead, the electron created on the conduction band of TiO_2 can be transferred into the conduction band of $ZnMn_2O_4$ and thereby it decreases the efficiency when both semiconductors are irradiated (figures 10a–b). In other words, $ZnMn_2O_4$ facilitates the electron and hole pair recombination and decreases the efficiency of the TiO_2. Figure 10a emphasizes the general protocol for the degradation of the pollutant when TiO_2 is coupled with a suitable semiconductor in the presence of UV–Vis light. Our data has some similarity with those on bulk $ZnMn_2O_4$ (Bessekhaud *et al* 2005).

4. Conclusions

Zinc manganese oxide ($ZnMn_2O_4$) nanoparticles were successfully prepared from the oxalate precursors of zinc and manganese obtained by the reverse micellar as well as the coprecipitation methods. Both the methods yield monophasic and uniform compositionally agglomerated nanoparticles. The average particle size of $ZnMn_2O_4$

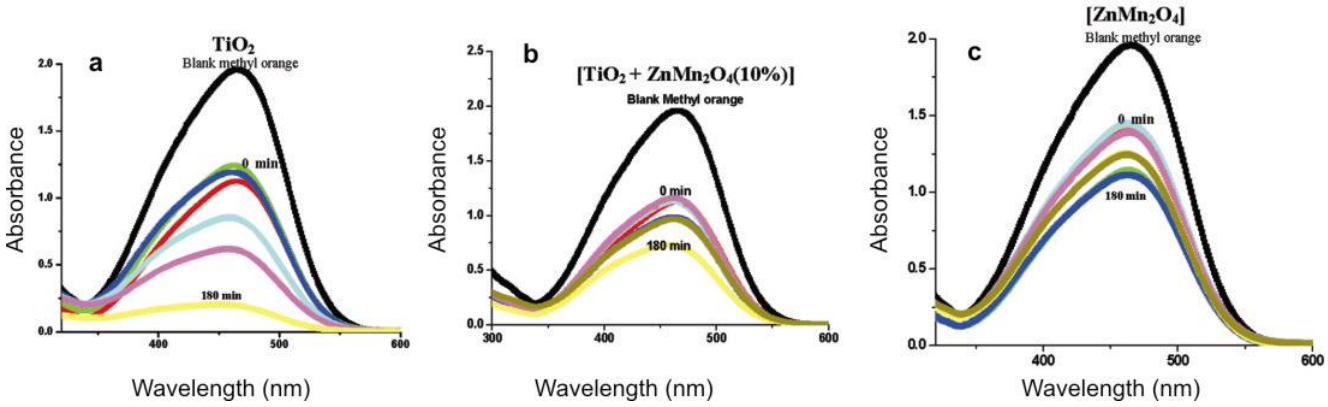

Figure 9. UV-Vis spectra showing the degradation of methyl orange under UV light using **a**. TiO_2, **b**. mixture of TiO_2 and $ZnMn_2O_4$ and **c**. $ZnMn_2O_4$.

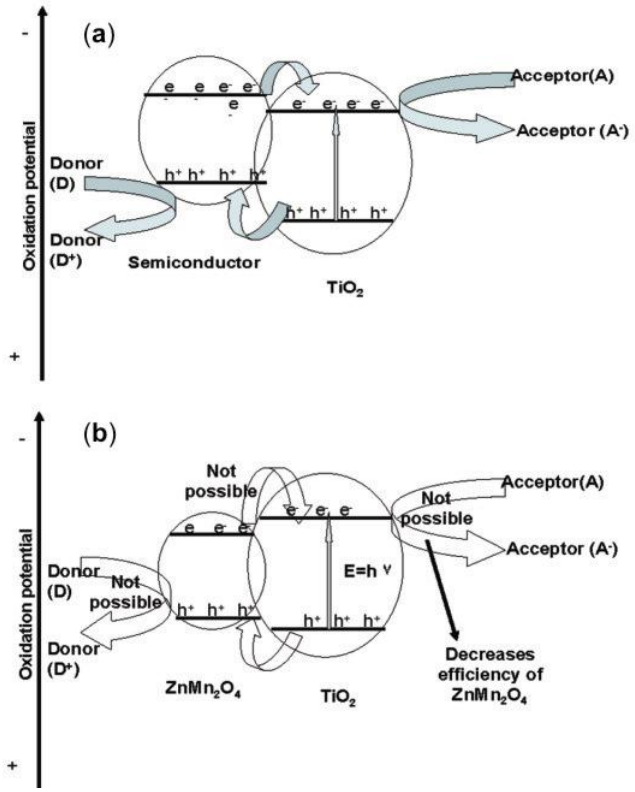

Figure 10. General energy diagram of **a**. coupled (TiO_2 + semiconductor) and **b**. $TiO_2 + ZnMn_2O_4$ for the photocatalytic oxidation reaction of the organic pollutant in the presence of UV light.

obtained from the reverse micellar method was in the range of 20–30 nm which is much smaller than that obtained by coprecipitation route (40–50 nm). Magnetization data shows a broad transition to antiferromagnetic order in the vicinity of ~150 K. Photocatalytic studies have also been performed which is in close agreement with that of bulk material.

Acknowledgements

Two of the authors (AKG) and (MQ) thank the Department of Science & Technology, Govt. of India and CSIR, Govt. of India for financial support. (KVR) acknowledges the receipt of CP-STIO award from the Department of Science and Technology, Government of India. Menaka thanks UGC, Govt. of India for a fellowship. (SEL) acknowledges support by NSF MRSEC DMR 0520471.

References

Ahmad T, Ramanujachary K V, Lofland S E and Ganguli A K 2004 *J. Mater. Chem.* **14** 3406

Ahmad T, Vaidya S, Sarkar N, Ghosh S and Ganguli A K 2005 *Nanotechnology* **17** 1236

Aiyama Y 1966 *J. Phys. Soc. Jpn* **21** 1684

Asbrink S, Waskowska A, Gerward L, Olsen J S and Talik E 1999 *Phys. Rev.* **B60** 12651

Bessekhaud Y, Robert D and Weber J V 2005 *Catal. Today* **101** 315

Chhor K, Bocquet J F and Pommier C 1986 *J. Chem. Thermodyn.* **18** 89

El-Aiashy M K, Mazhar H S and Kamal S M 1995 *Mater. Lett.* **24** 97

Fang J, Wang J, Gan L M, Chew C H and Ng S C 1997 *Nanostruct. Mater.* **8** 499

Feltz A and Jager M 1988 *Reactivity of Solids* **6** 119

Fritsch S G, Chanel C, Sarrias J, Bayonne S, Rausset A, Alcobe X and Sarrio M L M 2000 *Solid State Ionics* **128** 233

Ganguli A K, Ahmed J, Vaidya S and Ahmad T 2007 *J. Nanosci. Nanotechnol.* **7** 1760

Kuiry S C and Seal S 2004 *Encyclopedia of nanoscience and nanotechnology* (ed.) H S Nalwa (CA, USA: American Scientific Publishers) p. 369

Luisi P L and Straub B E 1984 *Reverse micelles* (New York: Plenum)

Monros G, Carda J, Tena M A, Escribano P, Badenes J and Cordoncillo E 1995 *J. Mater. Chem.* **5** 85

Peiteado M, Caballero A C and Makovec D 2007 *J. Solid State Chem.* **180** 2459
Qamar M *et al* 2008 *Catal. Today* **131** 3
Rosenberg M, Nicolau P, Manaila R and Pausescu P 1963 *J. Phys. Chem. Solids* **24** 1419
Sorita R and Kawano T 1996 *Sensor and Actuators* **B35–36** 274
Yang H, Yang Q H, Lu Y L and Li B X 1996 *J. Power Sources* **62** 223
Zhang X D, Wu Z S, Zang J, Li D and Zhang Z D 2007 *J. Phys. Chem. Solids* **68** 1583